NeuroImage: Clinical 36 (2022) 103229

Contents lists available at ScienceDirect

NeuroImage: Clinical

journal homepage: www.elsevier.com/locate/ynicl

Reduced coupling between the global blood-oxygen-level-dependent signal and cerebrospinal fluid inflow is associated with the severity of small vessel disease

Yao Zhang [a,1], Ruiting Zhang [a,b,1], Shuyue Wang [a], Hui Hong [a], Yeerfan Jiaerken [a], Kaicheng Li [a], Qingze Zeng [a], Xiao Luo [a], Xinfeng Yu [a], Minming Zhang [a,*], Peiyu Huang [a,*]

[a] Department of Radiology, The Second Affiliated Hospital, Zhejiang University School of Medicine, 310000 Hangzhou, China
[b] Department of Neurology, The Second Affiliated Hospital, Zhejiang University School of Medicine, 310000 Hangzhou, China

ARTICLE INFO

Keywords:
Cerebral small vessel disease
gBOLD-CSF coupling
CSF dynamics
Perivascular space

ABSTRACT

Background: Small vessel disease (SVD) is highly prevalent in the elderly and associated with an increased risk of dementia and stroke. SVD may have disturbed cerebrospinal fluid (CSF) flow, which can compromise waste clearance and accelerate disease progression.
Methods: We retrospectively included 146 SVD patients from a prospectively collected dataset, with one- or two-year follow-up data in 61 patients. The coupling strength between the global blood-oxygen-level-dependent (gBOLD) signal and CSF inflow was used to reflect CSF dynamics. We performed regression analyses to investigate the association between the gBOLD-CSF coupling index and the severity of SVD and vascular risk factors. Longitudinal analysis was carried out to investigate causal relationships.
Results: Patients with severe SVD had significantly decreased gBOLD-CSF coupling ($\beta = -0.180$, $p = 0.032$). Dilation of perivascular spaces in the basal ganglia area ($\beta = -0.172$, $p = 0.033$) and diabetes ($\beta = -0.204$, $p = 0.014$) were associated with reduced gBOLD-CSF coupling. In longitudinal analyses, diabetes was associated with faster decline in gBOLD-CSF coupling ($\beta = 0.20$, $p = 0.039$), while perivascular space (PVS) dilation in the centrum semiovale showed a opposite relationship ($\beta = -0.20$, $p = 0.041$). The gBOLD-CSF coupling could not predict SVD progression.
Conclusion: Altered CSF flow is associated with the severity of SVD.

1. Introduction

Small vessel disease (SVD) is common in elders. It is associated with a>2-fold increased risk of stroke (Wardlaw et al., 2013a) and nearly 50 % of dementia worldwide (Bos et al., 2018). Nevertheless, the prevention and treatment of SVD are facing difficulties due to its unclear pathological mechanisms (Bath and Wardlaw, 2015; Pantoni, 2010). Recent studies showed that impairment of the glymphatic system may contribute to the initiation and progression of SVD (Benveniste and Nedergaard, 2021; Zhang et al., 2021). As an upstream process, abnormal cerebrospinal fluid (CSF) flow could also lead to impaired waste clearance. In subjects with CSF circulation disorders, fluid stagnation can lead to severe brain damage and clinical symptoms (Bothwell et al., 2019; Eide et al., 2021). One study in SVD showed that altered CSF stroke volume at the foramen magnum was related to disease severity (Blair et al., 2020). However, this mechanism still needs further validation, especially from longitudinal analyses.

Interestingly, fluctuations in global cerebral blood volume due to low-frequency (<0.1 Hz) intrinsic vasomotor contractions or neural activities can cause large CSF flow (Fultz et al., 2019), which is believed to be due to intracranial pressure changes. This phenomenon could be detected *in vivo* by measuring the coupling between global blood volume (reflected by global blood-oxygen-level-dependent signal, gBOLD) and CSF inflow (reflected by inflow-related image enhancement) (Fultz et al., 2019). Studies confirmed that this gBOLD-CSF coupling exists either during sleep (Fultz et al., 2019) or wakefulness (Yang et al.,

* Corresponding authors at: Department of Radiology, The Second Affiliated Hospital, Zhejiang University School of Medicine, No.88 Jiefang Road, Shangcheng District, Hangzhou 310009, China.
E-mail addresses: zhangminming@zju.edu.cn (M. Zhang), huangpy@zju.edu.cn, zhangminming@zju.edu.cn, huangpy@zju.edu.cn (P. Huang).
[1] These authors contributed equally to this work.

https://doi.org/10.1016/j.nicl.2022.103229
Received 23 June 2022; Received in revised form 10 October 2022; Accepted 10 October 2022
Available online 12 October 2022

2022), and it has a much larger effect on CSF inflow compared to cardiac pulsation during wakefulness (Yang et al., 2022). Furthermore, altered coupling was found to be closely associated with pathological markers and clinical functions in patients with Parkinson's' disease (Han et al., 2021a) and Alzheimer's disease (Han et al., 2021b).

In the present study, we aim to investigate: (1) the association between SVD severity (including specific vascular factors) and gBOLD-CSF coupling; (2) the association between gBOLD-CSF coupling and cognitive impairments; (3) whether baseline gBOLD-CSF coupling could predict SVD progression and vice versa. We expect that gBOLD-CSF coupling would be associated with more severe SVD and cognitive decline.

2. Methods

2.1. Ethics approval

The study protocols were approved by the ethics committee of the 2nd Affiliated Hospital, Zhejiang University School of Medicine. All clinical investigation was conducted according to the principles expressed in the Declaration of Helsinki. All participants signed informed consent on admission.

2.2. Participants

We retrospectively reviewed the data of consecutive SVD patients (defined as the presence of lacunes and/or WMH on MRI) admitted to the neurology department of our hospital. The main reasons for referral to the hospital were acute (e.g. transient ischemic attack and stroke presenting with lacunar syndrome) or subacute symptoms of SVD (e.g. headache, cognitive and/or gait disturbances). The imaging data of patients with acute lacunar infarct were acquired at least six months after onset. The patients were invited to come back for yearly follow-ups. In this retrospective study, the inclusion criteria were as follows: (1) age $\geq$ 40; (2) having complete multi-modal MRI data, including T1-weighted (T1W) images, axial T2 fluid-attenuated inversion recovery (T2 FLAIR) images, susceptibility-weighted images (SWI) and resting-state functional MRI (rsfMRI) images; (3) having cognitive assessments. Exclusion criteria were as follows: (1) any other imaging evidence of preexisting structural brain lesion (hemorrhage, cerebral trauma, cerebrovascular malformation, brain tumors, etc.); (2) diagnosed with other neurological or psychiatric diseases.

2.3. Vascular risk factor assessment

Demographic and clinical information was collected from all subjects, including age, sex, history of alcohol drinking, smoking status, diabetes mellitus, hypertension, hyperlipidemia, and hyperhomocysteinemia. Smoking and drinking status were determined according to the subjects' self-report. Diabetes mellitus was defined as the presence of any of the following: fasting serum glucose $>$ 7.0 mmol/L or postprandial 2 h plasma glucose $>$ 11.1 mmol/L or having a previous history of diabetes. Hypertension was defined as the presence of any of the following: systolic blood pressure $\geq$ 140 mmHg or diastolic pressure $\geq$ 90 mmHg measured twice in quiet conditions or having a self-reported history of hypertension. Hyperlipidemia was defined as self-reported hyperlipidemia, or treatment with anti-dyslipidemia medication, fasting total cholesterol $>$ 5.2 mmol/l, or low-density lipoprotein $>$ 3.36 mmol/l. Hyperhomocysteinemia was defined as the presence of any of the following: fasting plasma total cysteine concentration $>$ 15 mmol/L or having a self-reported history of Hyperhomocysteinemia.

2.4. Neuropsychological assessment

Neuropsychological assessments were performed for all subjects (Supplemental materials eTable 1), covering global cognition (Montreal cognitive assessment, MoCA; mini-mental state examination, MMSE), executive function (Digit Symbol Substitution Test, DSST; Trail Making Test A, TMTA; Trail Making Test B, TMTB) and short-term memory (Digital Span Test, DST).

2.5. Image acquisition

All patients were scanned on a 3.0 Tesla MR scanner (General Electric Medical System, Discovery MR 750). T1W images, axial T2 FLAIR images (November 2013 – August 2020), 3D T2 FLAIR images (August 2020 – December 2020), SWI, and rsfMRI images were acquired. The T1W images were acquired with a 3D fast spoiled gradient-echo sequence, and the parameters were: TR = 7.3 ms; TE = 3.0 ms; flip angle = 8°; Inversion time (TI) = 450 ms; field of view = 250*250 mm^2; voxel size = 0.98*0.98*1mm^3; 164 sagittal slices. The parameters of axial T2 FLAIR were: TR = 8400 ms; TE = 150 ms; IR = 2,100 ms; field of view = 240*240 mm^2; voxel size = 0.47*0.47*4 mm^3; 36 axial slices. The 3D T2 FLAIR images were acquired using a CUBE sequence: the parameters were: TR = 5000 ms; TE = 128 ms; IR = 1612 ms; field of view = 256*256 mm^2; voxel size = 1*1*1mm^3; 176 sagittal slices. The SWI images were acquired using a 3D gradient echo sequence, the parameters were: TR = 33.8 s; first TE = 4.5 s; 8 echoes; flip angle = 20°; field of view = 240*240 mm^2; voxel size = 0.47*0.47*2mm^3; 60 axial slices. The rsfMRI was acquired using a gradient recalled echo/echo planar imaging sequence, the parameters were: TR = 2 s; TE = 30 ms; 180 volumes; flip angle = 77°; field of view = 240*240 mm^2; voxel size = 3.75*3.75*4mm^3; slice gap = 1 mm; 38 axial slices. The patients were asked to close their eyes and avoid sleep during the scan, confirmed afterward.

2.6. Assessment of SVD markers

All imaging markers of SVD were defined according to the Standards for Reporting Vascular Changes on Neuroimaging (STRIVE) (Wardlaw et al., 2013b). Lacunes were defined as round or ooid hypointense lesions on T1W images with corresponding hypointense lesions with a hyperintense rim on FLAIR images ranging from 3 to 15 mm. Cerebral microbleeds were classified as small, round, or ovoid hypointense lesions on SWI. Dilated perivascular spaces (dPVS) were defined as round, oval, or linear-shaped lesions with a signal intensity equal to CSF on T1W images, and we also examined FLAIR images to distinguish them from chronic lacunar infarcts. The severity of dPVS in the basal ganglia (BG) and centrum semiovale (CSO) areas was rated using a previously established 4-points scoring method (Zhu et al., 2011). White matter hyperintensity (WMH) was graded according to the Fazekas scale.

The volume of WMH was quantified by automatic segmentation using the Lesion Segmentation Tool toolbox (https://www.applied-statistics.de/lst.html) based on Statistical Parametric Mapping 12. To avoid the possible bias caused by different voxel sizes, we reconstructed the 3D FLAIR images and 2D FLAIR images to the same spatial resolution of 1*1*4 mm^3 and used the lesion prediction algorithm (LPA) (Schmidt, 2017, chap. 6.1) to perform lesion segmentation. The automatically created WMH mask images were then visually inspected and manually corrected by YZ. WMH was normalized (WMH_{norm}) by ICV (calculated using CAT12, https://neuro-jena.github.io/cat/) to remove the effect of head size.

Finally, we calculated the SVD total score to reflect the overall disease burden. One score was awarded for any of the following conditions: one or more lacunars, one or more microbleeds, moderate to severe (grades 2 $\sim$ 4) dPVS in the basal ganglia area (msBG-PVS), periventricular WMH Fazekas 3 (extending into the deep white matter) and/or deep WMH 2 $\sim$ 3 (early confluent or confluent)(Staals et al., 2014).

2.7. Coupling between gBOLD signal and CSF signal analysis

2.7.1. fMRI image preprocessing

All rsfMRI data were preprocessed with using the Data processing & Analysis of Brain Imaging toolbox (DPABI, version 6.0, https://rfmri.org/dpabi) based on the Statistical parametric Mapping 12 (SPM12; www.fil.ion.ucl.ac.uk/spm). The first 10 rsfMRI volumes were discarded to allow for the magnetization to reach a steady state. The remaining images were corrected for timing differences in slice acquisition and realigned for head motion. Then we removed the linear temporal trends and performed spatial smooth using a 4 mm full width at half maximum kernel. Then temporal filtering (band-pass filter, 0.01–0.1 Hz) was applied.

The realigned fMRI data were then skull-stripped and registered to the 152-brain Montreal Neurological Institute (MNI-152) space using FLIRT (linear registration) in FSL (FMRIB Software Library, v6.0, https://fsl.fmrib.ox.ac.uk/fsl/fslwiki/). The transformation matrix was saved for further analysis. Quality checks were performed to ensure the accuracy of co-registration by one rater (YZ). We skipped the routine nuisance regression of global signal, CSF signal, and motion parameters to avoid loss of crucial hemodynamic information, as demonstrated by a recent study (Fultz et al., 2019).

2.7.2. Definition of regions of interest (ROI)

Consistent with previous studies (Fultz et al., 2019; Han et al., 2021a, 2021b), the ROI of the cortical gray matter was defined based on the Harvard-Oxford cortical structural atlases. To avoid registration-induced signal loss, we transformed the ROI in the MNI-152 space back to each subject's imaging space. The ROI for measuring CSF inflow was defined on the bottom slices of fMRI images (near the bottom of the cerebellum), because they were most sensitive to the CSF inflow effect (Fultz et al., 2019). We manually drew the CSF ROIs on functional images, and its anatomic location was further confirmed on T1 images, which were co-registered with functional images (Fig. 1).

2.7.3. Calculation of the coupling between gBOLD signal and CSF signal

The CSF signals were extracted from the images before smoothing, and the gBOLD signals were extracted from the images before normalization, as described in previous studies (Han et al., 2021a,b). The time series were first Z-normalized and then spatially averaged across all voxels within the ROI. Cross-correlation between the gBOLD signal and CSF signal was computed using MATLAB. We set the BOLD signal as the reference and calculated the maximal cross-correlation over a range of time lags (−20 s to 20 s) for each patient. BOLD oscillations were demonstrated to be earlier than CSF flow oscillations (Piechnik et al., 2009), and the CSF signal had a strong anticorrelatio n with gBOLD signal at positive lag times (Fultz et al., 2019; Han et al., 2021a,b). We used the maximal anticorrelation for quantifying the strength of gBOLD-CSF coupling. To demonstrate that the oscillation of CBV would lead to the CSF inflow, we calculated the cross-correlation between the negative derivative of the gBOLD signal and the CSF signal like in previous studies. Because the coupling index was negative, to help better understand the result, the opposite of gBOLD-CSF coupling was used in further analyses. Therefore, a larger gBOLD-CSF coupling reflects a better association between glo bal brain activity and CSF flow.

2.7.4. Validation of the coupling index

To verify the credibility of the gBOLD-CSF coupling, we shuffled the gBOLD time series and CSF time series randomly across patients and calculated the coupling index. It was repeated 10,000 times to build a null distribution function. Finally, the p-value was calculated from the percentiles of this null distribution (Han et al., 2021a,b).

To investigate the potential effect of head motion on the calculation of the gBOLD-CSF coupling, we used framewise displacement, a composite index measuring translational and rotational motions (Yoo et al., 2005), to quantify individual head motion. Arousal fluctuation may also confound the gBOLD-CSF coupling to a large extent. To assess its influence, we calculated the standard deviation (SD) of the gBOLD signal to quantify arousal fluctuation. Previous studies have shown that a large value suggests a drowsy and sleepy state (Wong et al., 2013).

2.8. Statistical analysis

Statistical analysis was performed with the Statistical Package of Social Science (IBM SPSS Statistics 25). To avoid the influence of outliers, we excluded subjects who had a framewise displacement index or drowsy index of more than three standard deviations. The whole group was divided into two groups (SVD-light and SVD-severe group) according to the median SVD total score. Kolmogorov-Smirnov test was performed to assess data normality.

Firstly, to explore the associations between the gBOLD-CSF coupling and possible confounding factors (age, sex, framewise displacement, and drowsy index), we used Spearman's correlation analysis for continuous data and Student's *t*-test for binary variables.

Secondly, we aimed to investigate the association between the gBOLD-CSF coupling and SVD features. (1) Group difference in the gBOLD-CSF coupling was examined using a multiple linear regression model controlling for age and sex. (2) We investigated the association between vascular risk factors and gBOLD-CSF coupling (model 1). To identify the variables with independent contributions, we used multiple regression analysis with variable selections (forward and backward). We set the vascular risk factors (hypertension, diabetes, hyperlipemia, hyperhomocysteinemia, alcohol drinking, and smoking), age, and sex as independent variables, and set the gBOLD-CSF coupling as the dependent variable. (2) Then we investigated the association between SVD imaging markers and gBOLD-CSF coupling (model 2). The model was the same as model 1, except that we changed the vascular risk factors to SVD imaging markers (WMH_{norm}, presence of microbleeds, presence of

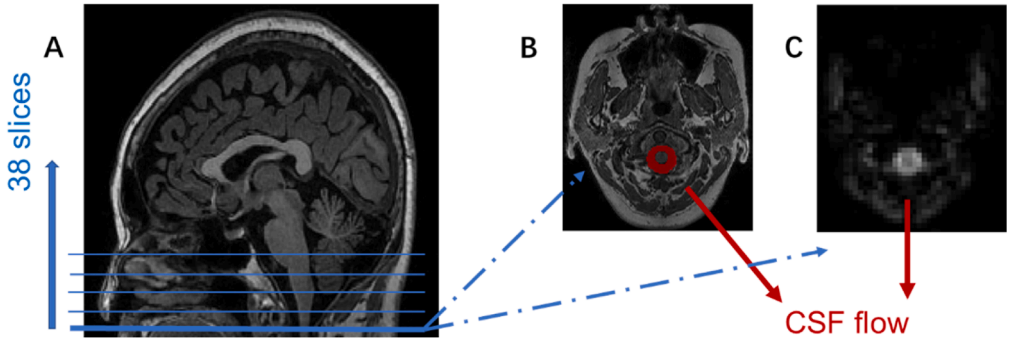

Fig. 1. The region for extracting CSF signal. (A) Example of scanning localization. The functional images were acquired from bottom to top (interleaved), with a total of 38 slices covering the whole brain. (B) and (C) were the bottom slice of the axial T1W and rsfMRI images. The red area was used to extract the CSF signal. (For interpretation of the references to colour in this figure legend, the reader is referred to the web version of this article.)

lacunes, and presence of msBG-PVS).

Thirdly, we examined the relationship between the gBOLD-CSF coupling and cognitive assessments. Similarly, we constructed linear regression models with each cognitive assessment score set as the dependent variable and the gBOLD-CSF coupling as the independent variable, controlling for age, sex, and education. Education was additionally included because it has an influence on both brain status and cognitive functions. As there were six cognitive domains, multiple comparison correction using the false discovery rate method was applied.

Finally, we analyzed the longitudinal data to investigate possible causal relationships between the gBOLD-CSF coupling and SVD markers. We examined: (1) whether baseline SVD imaging markers or vascular risk factors could predict the change of the gBOLD-CSF coupling over time, controlling for age, sex, and baseline coupling. Specifically, we calculated coupling_diff = (Coupling$_{_baseline}$ − Coupling$_{_followup}$)/time (year) to reflect its change rate. (2) whether baseline gBOLD-CSF coupling could predict SVD progression, controlling for age, sex, and baseline SVD features. The progression of lacunes or microbleeds was defined by the number of newly occurred lesions. The change in the PVS score was calculated by subtracting the follow-up score from the baseline score. The growth rate of WMH, WMH_{dev}, was calculated by the equation: WMH_{dev} = ($WMH_{norm\_followup}$ - $WMH_{norm\_baseline}$)/time (year). (3) The relationship between WMH_{dev} and coupling_diff. Similarly, multiple linear regression models were employed, with age, sex, and baseline gBOLD-CSF coupling included as covariates.

In all regression models, we used the variance inflation factor (VIF) to monitor multicollinearity. The VIFs should be ≤ 10 for the models to be valid.

3. Results

3.1. Demographics and SVD characteristics

We excluded one and three subjects due to drowsy state and severe head motion, respectively. Therefore, 146 participants went into final data analyses. Demographic and clinical data at baseline were reported in Table 1. The median age was 67 years, and 66 (45.2 %) were female. The median duration of education was 8 years. Among all subjects, 91 (62.3 %) had hypertension, 24 (16.4 %) had diabetes, 18 (12.3 %) had hyperlipidemia, 17 (11.6 %) had hyperhomocysteinemia, 28 (19.2 %) had a history of drinking and 39 (26.7 %) were smokers.

The whole sample was divided into SVD-light (SVD total score ≤ 2, n = 77) and SVD-severe (SVD total score > 2, n = 69) according to the median SVD total score (Table 1). The differences between the subgroups were shown in Table 1. Compared with the severe group, the light group had lower age ($p = 0.006$) and less hypertension ($p < 0.001$). The severe group had a more frequent presence of lacunes and microbleeds ($p < 0.001$), as well as higher BG-PVS scores and larger WMH_{norm} ($p < 0.001$).

A total of sixty-one participants had follow-up data. Compared with the those without longitudinal data (eTable 2), they had a younger age ($p = 0.04$), smaller WMH_{norm} ($p = 0.01$) and better execution functions (DSST, $p = 0.02$; TMTA, $p = 0.04$). At follow-up, thirteen subjects had new microbleeds, and four subjects had new lacunes. There was no change in BG-PVS and CSO-PVS scores (supplementary files eTable 3).

3.2. Validation of the CSF-gBOLD coupling

We found that there was a significant cross-correlation between the gBOLD signal and CSF signal for all participants. The gBOLD signal was significantly coupled to the CSF signal ($p < 0.001$ in all subjects; group mean $r = -0.344$; group mean lag = 6 s). Meanwhile, the negative first-order derivative of gBOLD signal were strongly correlated to the CSF signal ($p < 0.001$ in all subjects; group mean $r = -0.245$, group mean lag = −2s). As shown in a representative subject (Fig. 2), the CSF signal peaks often appeared during the fast-declining period of the gBOLD signal and lagged behind the gBOLD signal. In this subject, the most negative cross-correlation between the gBOLD and CSF signal is around 6 s lag (Fig. 2. B, $r = -0.562$, $p < 0.001$). Meanwhile, the max positive cross-correlation between the negative first-order derivative of the gBOLD signal and CSF signal is around −2s lag (Fig. 2. C, $r = 0.512$, $p <$

Table 1
Demographic, clinical and imaging data of baseline.

	SVD-total (n = 146)	SVD-light (n = 77)	SVD-severe (n = 69)	P value
Clinical profiles				
Age, y, median (IQR)	67 (61–73)	66 (57–71)	69 (63–75)	0.006
Female, n (%)	66 (45.2)	39 (50.6)	27 (39.1)	0.163
Education, y, median (IQR)	8 (3.7–11)	8 (3–12)	7 (4–7)	0.804
Alcohol drinking, n (%)	28 (19.2)	13 (16.5)	15 (22.5)	0.117
Smoking, n (%)	39 (26.7)	17 (21.5)	25 (35.2)	0.059
Hypertension, n (%)	91 (62.3)	36 (46.8)	55 (79.7)	<0.001
Diabetes, n (%)	24 (16.4)	9 (11.7)	15 (21.7)	0.113
Hyperlipidemia, n (%)	18 (12.3)	8 (10.1)	10 (14.5)	0.455
Hyperhomocysteinemia, n (%)	17 (11.6)	4 (5.1)	13 (18.8)	0.006
Cognitive assessments				
MMSE, median (IQR)	28 (23–29)	28 (25–29)	26 (22–28)	0.097
MOCA, median (IQR)	23 (17–26)	24 (19–27)	22 (15–25)	0.078
DSB, median (IQR)	10 (8–12)	11 (9–12)	9 (7–11)	0.011
DSST, mean (SD)	25 (15)	29 (15)	20 (13)	0.001
TMTA, second, median (IQR)	72.2 (46–98.5)	72.4 (48–95)	70 (44–117)	0.482
TMTB, second, mean (SD)	116 (81.4)	115 (69)	118 (94.4)	0.865
Radiological profiles				
Presence of lacunes, n (%)	74 (50.7)	9 (11.4)	65 (94.2)	<0.001
Presence of cerebral microbleeds, n (%)	62 (425)	11 (13.9)	51 (73.9)	<0.001
CSO-PVS, median (IQR)	2 (1–3)	2 (1–3)	2 (1–3)	0.610
BG-PVS, median (IQR)	3 (2–3)	2 (2–3)	3 (2–3)	<0.001
WMH_{norm}	0.009 (0.003–0.018)	0.003 (0.001–0.008)	0.017 (0.009–0.029)	<0.001
Coupling, mean (SD)	0.344 (0.157)	0.376 (0.178)	0.309 (0.122)	0.008

*P*p value < 0.05 was considered significant in comparison of the two subgroups (SVD-light vS SVD-severe).
Statistical results are reported as mean (standard deviation, SD) if the original data follows a normal distribution, otherwise as median (interquartile range, IQR).

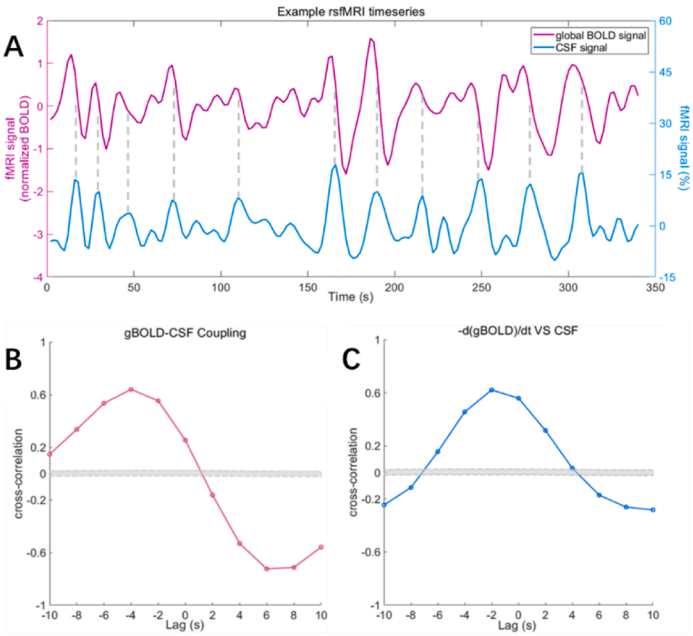

Fig. 2. Example of gBOLD-CSF coupling. (A) The gBOLD signal and CSF signal extracted from a representative subject showed synchronized trends in signal fluctuations. CSF inflow peaks often appeared during the fast-declining period of the gBOLD signal (dashed vertical lines). (B) The cross-correlation between gBOLD and CSF signals was the strongest at around 6 s. (C) The negative derivative of the gBOLD signal was also closely coupled to the CSF signal. The maximum was around −2s. Gray dashed lines in (B) and (C) represent the 95 % confidence interval of the null distribution. gBOLD signal: global blood-oxygen-level-dependent signal.

0.001). These results showed similar patterns to Fultz's study (Fultz et al., 2019).

3.3. Association between the gBOLD-CSF coupling and possible confounders

Correlations between the gBOLD-CSF coupling and head motion (r = −0.099, p = 0.23) and drowsiness index (r = 0.024, p = 0.77) were not significant. The gBOLD-CSF coupling was negatively correlated with the age (r = −0.180, p = 0.03). There was no significant difference between the females and males (p = 0.89).

3.4. Association between the gBOLD-CSF coupling and vascular features

After controlling for age and sex, we found that lower gBOLD-CSF coupling was associated with severe SVD (β = −0.180, p = 0.032). Regarding the contribution of individual SVD markers, the presence of severe msBG-PVS was independently associated with lower gBOLD-CSF coupling (β = −0.172, p = 0.03, R^2 = 8.3 %), while other SVD markers were excluded from the model. For vascular risk factors, only the presence of diabetes was related to lower gBOLD-CSF coupling (β = −0.200, p = 0.014, Table 2).

3.5. Association between the gBOLD-CSF coupling and cognition

As shown in Table 3, controlling for age, sex, and education, higher gBOLD-CSF coupling was significantly related to better DSST performance (β = 0.148, p = 0.038). There was no correlation between the gBOLD-CSF coupling and other cognitive assessments. The associations did not survive multiple comparison corrections.

Table 2
Associations between risk factors and SVD biomarkers and coupling.

	β value	*95 %CI*	P value
Age	−0.207	−0.006, 0.001	0.011
Sex	0.048	−0.033, 0.063	0.545
Diabetes	−0.200	−0.138, 0.016	0.014
msBG-PVS	−0.172	−0.176, 0.008	0.033

Abbreviations: msBG-PVS, moderate to severe (grades 2 ~ 4) dPVS in the basal ganglia area

Table 3
Associations between cognitive assessments and Coupling.

	Coupling		
	β value[a]	*95 %CI*	P value[a]
MMSE	0.052	−5.555, 10.510	0.544
MOCA	0.058	−4.940, 10.688	0.465
DSB	0.052	−2.707, 5.204	0.534
DSST	0.148	0.830, 27.759	0.038
TMTA	0.059	−42.489, 92.820	0.463
TMTB	−0.04	−99.5, 60.0	0.625

P value[a] < 0.05 are considered significant in multiple regression analysis adjusting for age, sex and education.
A higher TMTA/TMTB score indicates worse executive ability. For the rest of the cognitive assessments (MMSE, MOCA, DSB, DSST), a higher test score indicates better cognitive performance.

3.6. Longitudinal associations

Presence of diabetes at baseline was associated with a greater decrease in coupling (β = 0.20, p = 0.039, R^2 = 51.5 %), and baseline CSO-PVS score was associated with lower coupling_diff (β = −0.200, p = 0.041, Table 4). (2) There was no significant association between the baseline gBOLD-CSF coupling and WMH_{dev} (β = 0.066, p = 0.387). (3) There was no significant association between the coupling_diff and WMH_{dev} (β = −0.135, p = 0.279). Because there was almost no change in other SVD markers, they were not analyzed.

Table 4
Associations between risk factors and baseline SVD biomarkers and coupling_diff.

	β value	*95 %CI*	P value
Coupling	0.628	0.503, 0.962	0.000
Age	−0.117	−0.006, 0.002	0.249
Sex	−0.164	−0.129, 0.010	0.093
Diabetes	0.201	0.177, 0.159	0.039
CSO-PVS	−0.199	−0.001, 0.329	0.041

Abbreviations: CSO-PVS, centrum semiovale perivascular space.

4. Discussion

The present study explored the relationship between SVD and gBOLD-CSF coupling, a marker of CSF flow possibly linked to glymphatic clearance. We found that patients with severe SVD had reduced gBOLD-CSF coupling compared to mild cases. Decreased gBOLD-CSF coupling was found to be associated with advanced age, the presence of msBG-PVS, and the presence of diabetes. Higher gBOLD-CSF coupling was associated with better DSST performance. Furthermore, the presence of diabetes was significantly associated with a faster decline of gBOLD-CSF coupling, while the dilation of CSO-PVS showed the opposite effect. These findings may provide useful evidence for understanding the mechanism of SVD and improving clinical treatment.

Previously, most studies used phase-contrast MRI to investigate CSF flow (Blair et al., 2020; Eide et al., 2021). Recent functional brain imaging studies show that the drop of cerebral blood flow (CBF) and the related vacuum effect play a stunning role in CSF influx (Fultz et al., 2019), in agreement with the Monro-Kellie doctrine of constant intracranial volume (Mokri, 2001). The phenomenon has also been confirmed by a study using near-infrared spectroscopy (Borchardt et al., 2021). This mechanism may play a critical role in the sleep-related enhancement of CSF inflow (Fultz et al., 2019) and the occurrence of post-stroke edema (Mestre et al., 2020). Importantly, one recent study showed that in healthy awake participants, the low-frequency oscillations of gBOLD still largely outperform cardiac pulsatility——another important driving force (Yang et al., 2022). They suggested that vasomotion is the central physiology that underlies this processing. Notably, this phenomenon cannot be detected by traditional phase-contrast MRI due to its low temporal resolution.

We found that severe SVD patients had reduced gBOLD-CSF coupling. Many vascular and brain alterations could contribute to this abnormality, and we may get helpful information from the association between gBOLD-CSF coupling and each factor. Among all the SVD imaging markers, reduced coupling was associated with the dilation of BG-PVS, a marker consistently reported in imaging studies of SVD (Francis et al., 2019). Located downstream of CSF flow, the dPVS may reflect increased flow resistance and compensatory changes, as suggested by previous reviews (Brown et al., 2018; Wardlaw et al., 2020). Therefore, this may indicate coherent structural–functional changes linked by hydrokinetic principles. However, in longitudinal analysis, the dilation of CSO-PVS was associated with a slower decline in the coupling index. The reason for this inconsistency still needs further investigation.

Diabetes was associated with decreased gBOLD-CSF coupling and a faster gBOLD-CSF coupling decline rate. Indeed, previous studies found that diabetes was associated with both hydrocephalus (Räsänen et al., 2020) and SVD progression (Bernbaum et al., 2015). Our results further support their associations. It has been shown that advanced glycation end products (AGEs) related to diabetes might play crucial roles in this process (Rhee and Kim, 2018). The AGEs could promote inflammation and BBB destruction (Fishel et al., 2005) and cause PVS remodeling by releasing excess vascular endothelial growth factors (Jiang et al., 2017). In addition, diabetes may damage vascular smooth muscle cells (Nieves-Cintrón et al., 2021), leading to impaired v asomotion (Emerson and Segal, 2000) and decreased CSF driving forces.

Unexpectedly, hypertension was not associated with gBOLD-CSF coupling. It is possible that this coupling index is more sensitive to changes in temporal dynamics rather than amplitudes. Indeed, pulse-wave velocity rather than systolic blood pressure was found to be closely related to BOLD signal variance (Hussein et al., 2020). Although diabetes and hypertension could both impede fluid motion, their impacts on CSF hydrokinetics are distinct (Benveniste and Nedergaard, 2021). Further studies are needed to verify this result and to understand the exact pathophysiology.

The association between gBOLD-CSF coupling and cognitive performance was weaker than common SVD markers, and none of the results survived multiple comparison corrections. This could be understood because CSF circulation is a weak contributor to brain degeneration in most cases, except for severe hydrocephalus. Therefore, its association with behavioral changes might be weaker than parenchymal imaging markers, which reflect brain damage directly related to cognitive functions.

Several limitations of our study should be considered. Firstly, the sample size is relatively small and therefore would lead to statistical selection bias and lower power, especially in the longitudinal dataset. Although we invited subjects for annual follow-up indiscriminately, only a small part of them came back and the younger patients were more willing to participate, especially under the influence of the COVID-19 pandemic. These results still need to be validated in larger samples with longer follow-up times. Secondly, the association between the gBOLD-CSF coupling and cognitive assessments did not survive multiple comparison corrections and needs to be considered when interpreting the results. Thirdly, the spatial and temporal resolution of the fMRI data was not as high as in the original Fultz's study (Fultz et al., 2019). Nevertheless, this is not a severe issue due to: (1) The mechanism behind the gBOLD-CSF coupling during awake was suggested to be vasomotion (Yang et al., 2022), which has a period of about 20 s. Therefore, the 2-seconds TR is acceptable. (2) The whole gray matter was a large area, and the extracted BOLD signals were relatively robust to partial volume effect. On the other hand, the intensity of the CSF signal depends on the inflow effect but not on adjacent static tissues. Indeed, previous studies (Han et al., 2021a,b) using similar TRs (2 or 3 s) and voxel size successfully verified the gBOLD-CSF coupling and found its association with clinical features. Future studies utilizing multi-band data acquisition methods may provide better spatial specificity and more accurate coupling measurement. Fourthly, the fMRI data were acquired during the awake state when the coupling strength is relatively weak. Performing a study during the sleep state may provide more robust results. Finally, the association between gBOLD-CSF coupling and glymphatic clearance still needs further validation.

CRediT authorship contribution statement

Yao Zhang: Writing – original draft, Formal analysis, Validation. **Ruiting Zhang:** Writing – original draft, Data curation, Writing – review & editing. **Shuyue Wang:** Data curation. **Hui Hong:** Data curation. **Yeerfan Jiaerken:** Data curation. **Kaicheng Li:** Data curation. **Qingze Zeng:** Data curation. **Xiao Luo:** Data curation. **Xinfeng Yu:** Data curation. **Minming Zhang:** Conceptualization. **Peiyu Huang:** Conceptualization, Supervision, Writing – review & editing.

Declaration of Competing Interest

The authors declare that they have no known competing financial interests or personal relationships that could have appeared to influence the work reported in this paper.

Data availability

Data will be made available on request.

Acknowledgments

This study was supported by the Natural Science Foundation of Zhejiang Province (Grant No. LSZ19H180001 and LQ20H180015), the National Natural Science Foundation of China (Grant Nos. 81571654 and 81771820), the China Postdoctoral Science Foundation (Grant No. 2019M662083) and the Zhejiang province Postdoctoral Science Foundation.

Appendix A. Supplementary data

Supplementary data to this article can be found online at https://doi.

org/10.1016/j.nicl.2022.103229.

References

Bath, P.M., Wardlaw, J.M., 2015. Pharmacological treatment and prevention of cerebral small vessel disease: a review of potential interventions. Int. J. Stroke 10, 469–478. https://doi.org/10.1111/ijs.12466.

Benveniste, H., Nedergaard, M., 2021. Cerebral small vessel disease: a glymphopathy? Curr. Opin. Neurobiol. 72, 15–21. https://doi.org/10.1016/j.conb.2021.07.006.

Bernbaum, M., Menon, B.K., Fick, G., Smith, E.E., Goyal, M., Frayne, R., Coutts, S.B., 2015. Reduced blood flow in normal white matter predicts development of leukoaraiosis. J. Cereb. Blood Flow Metabol. 35, 1610–1615. https://doi.org/10.1038/jcbfm.2015.92.

Blair, G.W., Thrippleton, M.J., Shi, Y., Hamilton, I., Stringer, M., Chappell, F., Dickie, D. A., Andrews, P., Marshall, I., Doubal, F.N., Wardlaw, J.M., 2020. Intracranial hemodynamic relationships in patients with cerebral small vessel disease. Neurology 94, E2258–E2269. https://doi.org/10.1212/WNL.0000000000009483.

Borchardt, V., Korhonen, V., Helakari, H., Nedergaard, M., Myllylä, T., Kiviniemi, V., 2021. Inverse correlation of fluctuations of cerebral blood and water concentrations in humans. Eur. Phys. J. Plus 136, 497. https://doi.org/10.1140/epjp/s13360-021-01480-2.

Bos, D., Wolters, F.J., Darweesh, S.K.L., Vernooij, M.W., de Wolf, F., Ikram, M.A., Hofman, A., 2018. Cerebral small vessel disease and the risk of dementia: a systematic review and meta-analysis of population-based evidence. Alzheimers Dement 14, 1482–1492. https://doi.org/10.1016/j.jalz.2018.04.007.

Bothwell, S.W., Janigro, D., Patabendige, A., 2019. Cerebrospinal fluid dynamics and intracranial pressure elevation in neurological diseases. Fluids Barriers CNS 16, 9. https://doi.org/10.1186/s12987-019-0129-6.

Brown, R., Benveniste, H., Black, S.E., Charpak, S., Dichgans, M., Joutel, A., Nedergaard, M., Smith, K.J., Zlokovic, B.V., Wardlaw, J.M., 2018. Understanding the role of the perivascular space in cerebral small vessel disease. Cardiovasc. Res. 114, 1462–1473. https://doi.org/10.1093/CVR/CVY113.

Eide, P.K., Valnes, L.M., Lindstrøm, E.K., Mardal, K.-A., Ringstad, G., 2021. Direction and magnitude of cerebrospinal fluid flow vary substantially across central nervous system diseases. Fluids Barriers CNS 18, 16. https://doi.org/10.1186/s12987-021-00251-6.

Emerson, G.G., Segal, S.S., 2000. Electrical coupling between endothelial cells and smooth muscle cells in hamster feed arteries: role in vasomotor control. Circul. Res. 87, 474–479.

Fishel, M.A., Watson, G.S., Montine, T.J., Wang, Q., Green, P.S., Kulstad, J.J., Cook, D.G., Peskind, E.R., Baker, L.D., Goldgaber, D., Nie, W., Asthana, S., Plymate, S.R., Schwartz, M.W., Craft, S., 2005. Hyperinsulinemia provokes synchronous increases in central inflammation and beta-amyloid in normal adults. Arch. Neurol. 62, 1539–1544.

Francis, F., Ballerini, L., Wardlaw, J.M., 2019. Perivascular spaces and their associations with risk factors, clinical disorders and neuroimaging features: a systematic review and meta-analysis. Int. J. Stroke 14, 359–371. https://doi.org/10.1177/1747493019830321.

Fultz, N.E., Bonmassar, G., Setsompop, K., Stickgold, R.A., Rosen, B.R., Polimeni, J.R., Lewis, L.D., 2019. Coupled electrophysiological, hemodynamic, and cerebrospinal fluid oscillations in human sleep. Science 366, 628–631. https://doi.org/10.1126/science.aax5440.

Han, F., Brown, G.L., Zhu, Y., Belkin-Rosen, A.E., Lewis, M.M., Du, G., Gu, Y., Eslinger, P. J., Mailman, R.B., Huang, X., Liu, X., 2021a. Decoupling of global brain activity and cerebrospinal fluid flow in parkinson's disease cognitive decline. Movement Disorders 36, 2066–2076. https://doi.org/10.1002/mds.28643.

Han, F., Chen, J., Belkin-Rosen, A., Gu, Y., Luo, L., Buxton, O.M., Liu, X., 2021b. Reduced coupling between cerebrospinal fluid flow and global brain activity is linked to Alzheimer disease-related pathology. PLoS Biol. 19, e3001233 https://doi.org/10.1371/journal.pbio.3001233.

Hussein, A., Matthews, J.L., Syme, C., Macgowan, C., MacIntosh, B.J., Shirzadi, Z., Pausova, Z., Paus, T., Chen, J.J., 2020. The association between resting-state functional magnetic resonance imaging and aortic pulse-wave velocity in healthy adults. Hum. Brain Mapp. 41, 2121–2135. https://doi.org/10.1002/hbm.24934.

Jiang, Q., Zhang, L., Ding, G., Davoodi-Bojd, E., Li, Q., Li, L., Sadry, N., Nedergaard, M., Chopp, M., Zhang, Z., 2017. Impairment of the glymphatic system after diabetes. J. Cereb. Blood Flow Metabol. 37, 1326–1337. https://doi.org/10.1177/0271678X16654702.

Mestre, H., Du, T., Sweeney, A.M., Liu, G., Samson, A.J., Peng, W., Mortensen, K.N., Stæger, F.F., Bork, P.A.R., Bashford, L., Toro, E.R., Tithof, J., Kelley, D.H., Thomas, J. H., Hjorth, P.G., Martens, E.A., Mehta, R.I., Solis, O., Blinder, P., Kleinfeld, D., Hirase, H., Mori, Y., Nedergaard, M., 2020. Cerebrospinal fluid influx drives acute ischemic tissue swelling. Science 367. https://doi.org/10.1126/science.aax7171.

Mokri, B., 2001. The Monro-Kellie hypothesis: applications in CSF volume depletion. Neurology 56, 1746–1748.

Nieves-Cintrón, M., Flores-Tamez, V.A., Le, T., Baudel, M.-M.-A., Navedo, M.F., 2021. Cellular and molecular effects of hyperglycemia on ion channels in vascular smooth muscle. Cell. Mol. Life Sci. 78, 31–61. https://doi.org/10.1007/s00018-020-03582-z.

Pantoni, L., 2010. Cerebral small vessel disease: from pathogenesis and clinical characteristics to therapeutic challenges. Lancet Neurol. 9, 689–701. https://doi.org/10.1016/S1474-4422(10)70104-6.

Piechnik, S.K., Evans, J., Bary, L.H., Wise, R.G., Jezzard, P., 2009. Functional changes in CSF volume estimated using measurement of water T2 relaxation. Magnet. Reson. Med. 61, 579–586. https://doi.org/10.1002/mrm.21897.

Räsänen, J., Huovinen, J., Korhonen, V.E., Junkkari, A., Kastinen, S., Komulainen, S., Oinas, M., Avellan, C., Frantzen, J., Rinne, J., Ronkainen, A., Kauppinen, M., Lönnrot, K., Perola, M., Koivisto, A.M., Remes, A.M., Soininen, H., Hiltunen, M., Helisalmi, S., Kurki, M.I., Jääskeläinen, J.E., Leinonen, V., 2020. Diabetes is associated with familial idiopathic normal pressure hydrocephalus: a case-control comparison with family members. Fluids Barriers CNS 17. https://doi.org/10.1186/S12987-020-00217-0.

Rhee, S.Y., Kim, Y.S., 2018. The role of advanced glycation end products in diabetic vascular complications. Diabetes Metab. J. 42, 188–195. https://doi.org/10.4093/dmj.2017.0105.

Schmidt, P., 2017. Bayesian inference for structured additive regression models for large-scale problems with applications to medical imaging. LudwigMaximilians-Universität München. https://doi.org/10.5282/edoc.20373.

Staals, J., Makin, S.D., Doubal, F.N., Dennis, M.S., Wardlaw, J.M., 2014. Stroke subtype, vascular risk factors, and total MRI brain small-vessel disease burden. Neurology 83, 1228–1234. https://doi.org/10.1212/WNL.0000000000000837.

Wardlaw, J.M., Benveniste, H., Nedergaard, M., Zlokovic, B. v., Mestre, H., Lee, H., Doubal, F.N., Brown, R., Ramirez, J., MacIntosh, B.J., Tannenbaum, A., Ballerini, L., Rungta, R.L., Boido, D., Sweeney, M., Montagne, A., Charpak, S., Joutel, A., Smith, K.J., Black, S.E., 2020. Perivascular spaces in the brain: anatomy, physiology and pathology. Nat Rev Neurol 16, 137–153. https://doi.org/10.1038/S41582-020-0312-Z.

Wardlaw, J.M., Smith, C., Dichgans, M., 2013a. Mechanisms of sporadic cerebral small vessel disease: insights from neuroimaging. Lancet Neurol. 12, 483–497. https://doi.org/10.1016/S1474-4422(13)70060-7.

Wardlaw, J.M., Smith, E.E., Biessels, G.J., Cordonnier, C., Fazekas, F., Frayne, R., Lindley, R.I., O'Brien, J.T., Barkhof, F., Benavente, O.R., Black, S.E., Brayne, C., Breteler, M., Chabriat, H., Decarli, C., de Leeuw, F.E., Doubal, F., Duering, M., Fox, N.C., Greenberg, S., Hachinski, V., Kilimann, I., Mok, V., Oostenbrugge, R., Pantoni, L., Speck, O., Stephan, B.C., Teipel, S., Viswanathan, A., Werring, D., Chen, C., Smith, C., van Buchem, M., Norrving, B., Gorelick, P.B., Dichgans, M., 2013b. Neuroimaging, S.T. for R.V. changes on, Neuroimaging standards for research into small vessel disease and its contribution to ageing and neurodegeneration. Lancet Neurol. 12, 822–838. https://doi.org/10.1016/S1474-4422(13)70124-8.

Wong, C.W., Olafsson, V., Tal, O., Liu, T.T., 2013. The amplitude of the resting-state fMRI global signal is related to EEG vigilance measures. Neuroimage 83, 983–990. https://doi.org/10.1016/j.neuroimage.2013.07.057.

Yang, H.-C.-S., Inglis, B., Talavage, T.M., Nair, V.V., Yao, J.F., Fitzgerald, B., Schwichtenberg, A.J., Tong, Y., 2022. Coupling between cerebrovascular oscillations and CSF flow fluctuations during wakefulness: an fMRI study. J. Cereb. Blood Flow Metabol. 271678X221074639 https://doi.org/10.1177/0271678X221074639.

Yoo, S.-S., Choi, B.-G., Juh, R., Pae, C.-U., Lee, C.-U., 2005. Head motion analysis during cognitive fMRI examination: application in patients with schizophrenia. Neurosci. Res. 53, 84–90.

Zhang, W., Zhou, Y., Wang, J., Gong, X., Chen, Z., Zhang, X., Cai, J., Chen, S., Fang, L., Sun, J., Lou, M., 2021. Glymphatic clearance function in patients with cerebral small vessel disease. Neuroimage 238, 118257. https://doi.org/10.1016/j.neuroimage.2021.118257.

Zhu, Y.C., Dufouil, C., Mazoyer, B., Soumaré, A., Ricolfi, F., Tzourio, C., Chabriat, H., 2011. Frequency and location of dilated Virchow-Robin spaces in elderly people: a population-based 3D MR imaging study. AJNR Am. J. Neuroradiol. 32, 709–713. https://doi.org/10.3174/ajnr.A2366.